Mechanical Engineering Advances 2024, 2(2), 463.
https://doi.org/10.59400/mea.v2i2.463

Article

Performance-based optimization of active-passive hybrid mass damper based on virtual TMD algorithm

Yu Yang[1], Qi Wang[2,*], Qingshan Yang[1], Tao Long[1], Guandong Qiao[2], Tian Li[1]

[1] School of Civil Engineering, Chongqing University, Chongqing 400044, People's Republic of China
[2] School of Civil and Architectural Engineering, Hainan University, Haikou 570228, People's Republic of China
*** Corresponding author:** Qi Wang, dkw57@hainanu.edu.cn

CITATION

Yang Y, Wang Q, Yang Q, et al. Performance-based optimization of active-passive hybrid mass damper based on virtual TMD algorithm. Mechanical Engineering Advances. 2024; 2(2): 463. https://doi.org/10.59400/mea.v2i2.463

ARTICLE INFO

Received: 14 May 2024
Accepted: 4 July 2024
Available online: 2 August 2024

Abstract: Subjecting structures to external forces inevitably leads to the generation of vibrations. For high-rise and flexible structures, excessive vibrations can significantly impact their normal operation and structural integrity. To mitigate these undesirable vibrations, structural vibration control is essential. Among various passive control methods, the tuned mass damper (TMD) is widely used for its ability to reduce vibrations through resonance with the structure. Meanwhile, the active mass damper (AMD) can also achieve an excellent control efficiency by exerting active control force on structures. Hybrid control integrates the benefits of multiple control strategies and applies the control forces on the same structure simultaneously. Hybrid mass damper (HMD) combines the passive characteristics of TMD and the active features of AMD, overcoming the limitations associated with using either system in isolation. This paper proposes a novel hybrid control method based on virtual TMD algorithm and optimizes the parameters of HMD by weighting the structural response and stroke of HMD to improve the comprehensive control performance. The effectiveness of this optimization is substantiated in the frequency domain. Additionally, numerical simulations are conducted to compare the optimized HMD with the traditional TMD and the unoptimized HMD, demonstrating both the effectiveness of the optimization and the superior control performance of the optimized HMD. The numerical results indicate that the optimized HMD reduces stroke by 15.6% compared to the unoptimized HMD on the premise that the control effect only loses 2.4%. Overall, the optimized HMD demonstrates superior comprehensive control performance relative to the unoptimized HMD.

Keywords: vibration control; active-passive hybrid mass damper; virtual tuned mass damper; weighted function; performance-based optimization; comprehensive control performance

1. Introduction

Actual engineering structures are located in complex environments and subjected to various loads. The excessive vibrations caused by the external loads may affect the normal service and safety of structures, especially for the high rise and flexible structures. Therefore, it is essential to control the structure's vibration to avoid excessive vibrational deformation that could impair its functionality. Structural vibration control is an effective measure to reduce the undesired vibrations of structures, and can be divided into passive, active, semi-active, and hybrid control [1] according to whether external energy output is required.

Tuned mass damper (TMD) is one of the most commonly used passive control methods in engineering, originating from a vibration device called dynamic vibration absorber (DVA) invented by Frahm in 1909 [2]. The TMD device consists of a mass block, spring and viscous damping. Owing to its straightforward structure and

economical cost, the TMD is extensively employed in practical engineering structures. For example, Tsai et al. and Rana et al. studied the optimal design parameters of TMD under harmonic and seismic excitations respectively [3,4]. TMD has a good control performance in the responses dominated by the fundamental frequency of structure and widely used in the vibration of high rise and flexible structures. For example, Murtagh et al. researched the control performance of TMD for vibration control of wind turbines under random wind loads [5]. Kim et al. studied the passive control of along wind response of tall building using TMD [6]. Dinh and Basu studied the application of TMD in vibration control of floating wind turbines [7]. When the natural frequency of TMD is tuned with the structure, it rapidly attenuates the dynamic response of the structure by resonating with the structure and dissipating energy through damping. Generally, when tuned with the structures, TMD has a good control performance in the fundamental frequency of structures.

Active mass damper (AMD) or active tuned mass damper (ATMD) can achieve an excellent control efficiency by exerting active control force on the structures [8–10]. When AMD or ATMD is integrated with suitable active control algorithms, the control effectiveness can surpass that of TMD, thus it is also extensively applied in practical engineering. For example, You et al. researched the along wind-induced vibration control using ATMD [8]. Fitzgerald et al. studied the vibration control of wind turbine towers using ATMD and demonstrated the improvements in structural reliability of the ATMD equipped wind turbine towers [9]. Cong adopted ATMD to simultaneously control the vibrations in wind turbine blades and tower and demonstrated that the ATMD has good control effect on blades and tower [10]. The main components of an active control system include controllers, sensors, and actuators. The controller is the key of the active control and AMD/ATMD combined with effective and reasonable controllers can achieve excellent control performance.

Semi-active control can reduce the vibrations of structures and maintain the tuning state by changing the stiffness or damping of control devices [11–17]. Compared to passive control, semi-active control is tunable and reduces the risk of detuning. When combined with suitable semi-active control algorithms, its effectiveness can rival that of active control. Consequently, numerous scholars have investigated different semi-active control devices and algorithms to achieve high-performance control. For example, Hrovat et al. studied the semi-active control of civil engineering structures and proposed rules for semi-active control systems to achieve the active control performance as much as possible [11]. Nagarajaiah and Varadarajan proposed a mechanical semi-active variable stiffness tuned mass damper to realize the semi-active control of high-rise buildings under wind loads [12]. Sun et al. applied magnetorheological elastomer in TMD to achieve the semi-active control and conducted an experiment under earthquake excitation [13]. Yang et al. also utilized the semi-active control characteristic of magnetorheological elastomer TMD to control the wind induced vibrations of constructing bridge towers [14]. Wang et al. utilized the variable stiffness and damping characteristics of semi-active control to reduce the earthquake and human induced vibrations [15–17]. Generally, semi-active control can change its own dynamic parameters to avoid the risk of detuning and can achieve excellent control performance with appropriate semi-active control algorithms.

Hybrid control contains the characteristics of two or more control measures, and

applies the control forces on the same structure simultaneously. The hybrid mass damper (HMD) combines the advantages of both TMD and AMD, and has attracted the attention of many scholars [18–20]. Li and Cao studied the application of HMD to attenuate the undesirable vibrations of structures under the ground acceleration [18]. Collette and Chesne proposed that adding an active control force between TMD and structure to make the TMD device a hybrid mass damper with active-passive characteristics [19]. Hsieh et al. combined TMD tuned to the fundamental frequency and tuned liquid damper (TLD) tuned to the forced frequency to form HMD and researched the control performance for offshore wind turbines [20]. HMD combines the advantages of TMD and AMD, and reduces the limitations of using TMD or AMD systems alone. Moreover, and the control effect of HMD is similar to that of active control and with lower energy consumption and power output requirements.

While TMD devices offer effective narrowband control, their performance is significantly compromised if detuning occurs due to changes in the structure's fundamental frequency. Although AMD and ATMD can deliver excellent control results, they necessitate substantial external energy input. Semi-active control techniques can provide continuous real-time tuning, but their range of tuning capability is also limited. The HMD combines the characteristics of both TMD and AMD, thereby minimizing the risk of detuning while maintaining robust control efficiency. Therefore, it is valuable to research the HMD in the structural vibration control.

This paper introduces an HMD device utilizing a virtual TMD control algorithm based on the vibration reduction principles of TMD and ATMD, and optimizes the design of the HMD by weighting the control effect and actuation stroke. Compared to existing HMD devices, the HMD device in this article aims to achieve the control effect of TMD devices with high mass ratios (≥5%) through the passive and active parts of the HMD without increasing the actual physical mass, where the passive part is the restoring force provided by stiffness and damping, and the active part is the active control force based on actuators. This paper first studied the hybrid control based on virtual TMD and validated the feasibility by frequency domain analysis. Then, this paper optimized the design parameters of HMD by considering the responses of structure and the stroke of control device in a weighted manner. Subsequently, the feasibility of the optimized design parameters was verified through numerical example. The results showed that the optimized HMD almost has the same control effect of the unoptimized HMD, while the stroke of the optimized HMD is much lower than that of the unoptimized HMD.

2. Hybrid control based on virtual TMD

TMD has good control performance in the responses of the fundamental frequency of structure and the control effect increases as the mass of TMD increases. While in actual engineering, the mass of TMD will be limited by the economy and installation space, which limits the control performance of TMD. This paper applies the control force of TMD with large mass onto structure to form AMD to improve the control effect without increasing the actual mass of control device. Afterwards, by replacing part of the control force with stiffness and damping, AMD is transformed

into HMD without changing the control effect to possess both active and passive control characteristics. The schematic diagram of SDOF structure with HMD is shown in **Figure 1**.

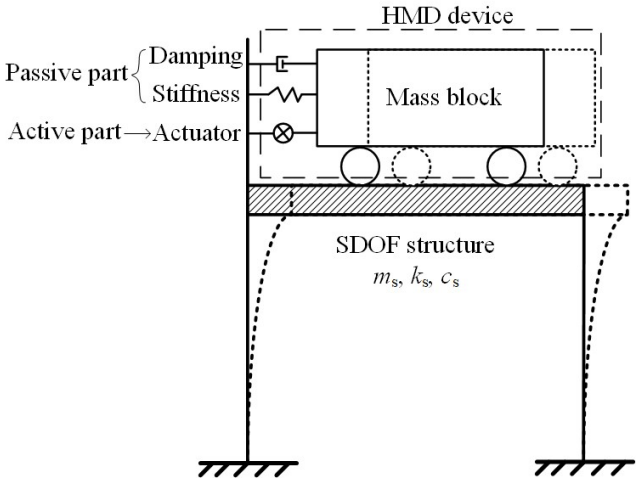

Figure 1. Schematic diagram of SDOF structure with HMD.

Assuming the mass of the single degree of freedom (SDOF) structure is m_s, the stiffness is k_s, and the damping is c_s. The total mass of the control device is m_t, the virtual mass of TMD is m_{vs}, the virtual stiffness is k_{vs}, and the virtual damping is c_{vs}.

The dynamic equation of the controlled SDOF structure is:

$$\begin{cases} m_s\ddot{x}_s + c_s\dot{x}_s + k_s x_s - f = p \\ m_t(\ddot{x}_s + \ddot{x}_t) + f = 0 \\ f = k_{vs}x_{vs} + c_{vs}\dot{x}_{vs} \end{cases} \tag{1}$$

The control equation of virtual TMD is:

$$\begin{cases} m_s\ddot{x}_s + c_s\dot{x}_s + k_s x_s - c_{vs}\dot{x}_{vs} - k_{vs}x_{vs} = p \\ m_{vs}(\ddot{x}_s + \ddot{x}_{vs}) + c_{vs}\dot{x}_{vs} + k_{vs}x_{vs} = 0 \end{cases} \tag{2}$$

Combining Equations (1) and (2), the expression of the control force can be obtained as:

$$f = \frac{k_{vs}m_t}{m_{vs}}x_t + \frac{c_{vs}m_t}{m_{vs}}\dot{x}_t - \left(k_{vs}\frac{m_{vs}-m_t}{m_{vs}}x_s + c_{vs}\frac{m_{vs}-m_t}{m_{vs}}\dot{x}_s\right) \tag{3}$$

From the expression of control force based on virtual TMD, the active control force based on the positive feedback of the relative state of the control device is similar to the control equation of TMD. Therefore, the control force can be replaced by stiffness and damping elements. The parameters of the stiffness and damping components for the replacement part are as follows.

$$k_t = \frac{k_{vs}m_t}{m_{vs}}; c_t = \frac{c_{vs}m_t}{m_{vs}} \tag{4}$$

The expression of the active force after replacement is:

$$f_{ac} = k_{vs}\frac{m_{vs}-m_t}{m_{vs}}x_s + c_{vs}\frac{m_{vs}-m_t}{m_{vs}}\dot{x}_s = ax_s + b\dot{x}_s \tag{5}$$

Then, the dynamic equation of SDOF structure controlled by HMD based virtual TMD is:

$$\begin{cases} m_s\ddot{x}_s + c_s\dot{x}_s + k_s x_s - k_t x_t - c_t\dot{x}_t + ax_s + b\dot{x}_s = p \\ m_t(\ddot{x}_s + \ddot{x}_t) + k_t x_t + c_t\dot{x}_t - ax_s - b\dot{x}_s = 0 \end{cases} \tag{6}$$

Denoting that $k_s/m_s = \omega_s^2$, $c_s/m_s = 2\xi_s\omega_s$, $a/m_s = \omega_{eq}^2$, $b/m_s = 2\xi_{eq}\omega_{eq}$, $k_t/m_t = \omega_t^2$, $c_t/m_t = 2\xi_t\omega_t$, $m_t/m_s = \mu$, $\omega_t/\omega_s = \upsilon$, $\omega/\omega_s = \lambda$, $\omega_{eq}/\omega_s = \gamma$, the transfer function of SDOF structural response controlled by HMD based virtual TMD can be obtained.

$$|H_s(i\omega)| = \frac{1}{k_s}\sqrt{\frac{(\upsilon^2-\lambda^2)^2+(2\xi_t\upsilon\lambda)^2}{\left\{\begin{bmatrix}(1+\gamma^2-\lambda^2)(\upsilon^2-\lambda^2)-4\xi_t\upsilon\lambda^2(\xi_s+\xi_{eq}\gamma)\\+\upsilon^2(-\gamma^2-\mu\lambda^2)+4\xi_t\xi_{eq}\upsilon\gamma\lambda^2\end{bmatrix}^2+\begin{bmatrix}2\xi_t\upsilon\lambda(1+\gamma^2-\lambda^2)+2\lambda(\xi_s+\xi_{eq}\gamma)(\upsilon^2-\lambda^2)\\-2\xi_{eq}\gamma\upsilon^2\lambda+2\xi_t\upsilon\lambda(-\gamma^2-\mu\lambda^2)\end{bmatrix}^2\right\}}} \tag{7}$$

The transfer function of HMD stroke is:

$$|H_t(i\omega)| = \sqrt{\frac{(\gamma^2/\mu+\lambda^2)^2+(2\xi_{eq}\gamma\lambda/\mu)^2}{(\upsilon^2-\lambda^2)^2+(2\xi_t\upsilon\lambda)^2}}|H_s(i\omega)| \tag{8}$$

The design parameters of TMD are set as follows:

$$\upsilon_{TMD} = \frac{1}{1+\mu}, \xi_{TMD} = \sqrt{\frac{3\mu}{8(1+\mu)^3}} \tag{9}$$

The design parameters of HMD based on virtual TMD are set as follows:

$$\upsilon = \frac{1}{1+\mu}, \xi_t = \sqrt{\frac{3\mu}{8(1+\mu)^3}}, \gamma = \frac{\sqrt{\mu_{vs}-\mu}}{1+\mu_{vs}}, \xi_{eq} = \sqrt{\frac{3\mu_{vs}(\mu_{vs}-\mu)}{8(1+\mu_{vs})^3}} \tag{10}$$

It can been that when $\mu = \mu_{vs}$, $\gamma = \xi_{eq} = 0$ and Equation (7) is the transfer function of TMD controlled SDOF structure. When $\mu = 0.01$, $\mu_{vs} = 0.05$ or 0.1, the amplitude of transfer functions of TMD and HMD controlled SDOF structural responses are displayed in **Figure 2**. The amplitude of transfer functions of TMD and HMD strokes are shown in **Figure 3**.

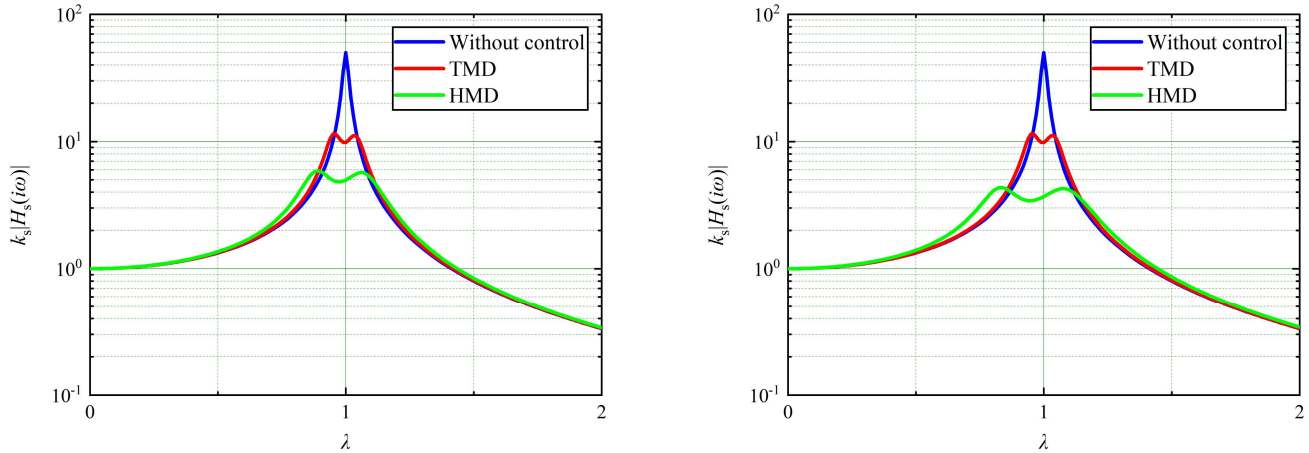

(a) $\mu = 0.01$, $\mu_{vs} = 0.05$. **(b)** $\mu = 0.01$, $\mu_{vs} = 0.1$.

Figure 2. Amplitudes of TMD and HMD controlled SDOF structural responses. **(a)** $k_s|H_s(i\omega)|$ with $\mu = 0.01$, $\mu_{vs} = 0.05$; **(b)** $k_s|H_s(i\omega)|$ with $\mu = 0.01$, $\mu_{vs} = 0.1$.

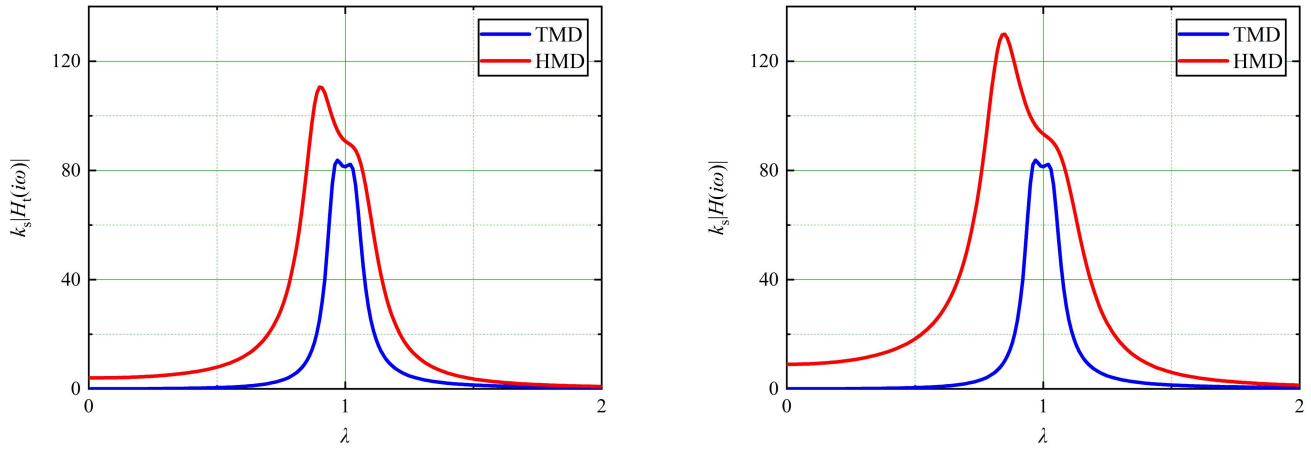

(a) $\mu = 0.01$, $\mu_{vs} = 0.05$. **(b)** $\mu = 0.01$, $\mu_{vs} = 0.1$.

Figure 3. Amplitudes of TMD and HMD strokes. **(a)** $k_s|H_t(i\omega)|$ with $\mu = 0.01$, $\mu_{vs} = 0.05$; **(b)** $k_s|H_t(i\omega)|$ with $\mu = 0.01$, $\mu_{vs} = 0.1$.

The results show that the HMD based on virtual TMD does not change the mass of device and realizes the improvement in control effect. The control performance of HMD based on virtual TMD increases with the increase of virtual mass ratio μ_{vs}, while the stroke will also increase. From Equations (7) and (8), it can be seen that the control performance and stroke of HMD are influenced by parameters γ, ξ_{eq}, υ and ξ_t. In order to balance the control performance and the stroke of HMD, the next chapter will optimize those parameters of HMD considering the structural response and the stroke in a weighted manner.

3. Optimization of hybrid mass damper

From the previous section, it can be seen that when μ and μ_{vs} are ascertained, the control effect of HMD is influenced by four parameters, i.e., active parameters (γ and ξ_{eq}) and passive parameters (υ and ξ_t). **Figures 4** and **5** give the influences of active parameters on the structural response and stroke of HMD. **Figures 6** and **7** give the influences of passive parameters on the structural response and stroke of HMD.

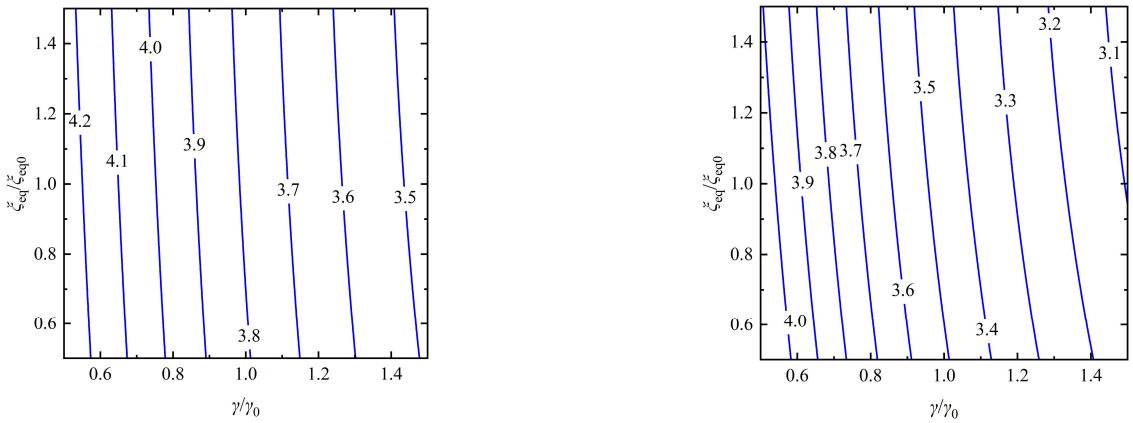

(a) $\mu = 0.01$, $\mu_{vs} = 0.05$. **(b)** $\mu = 0.01$, $\mu_{vs} = 0.1$.

Figure 4. Influences of active parameters on the structural response. **(a)** ξ_{eq}/ξ_{eq0} with $\mu = 0.01$, $\mu_{vs} = 0.05$; **(b)** ξ_{eq}/ξ_{eq0} with $\mu = 0.01$, $\mu_{vs} = 0.1$.

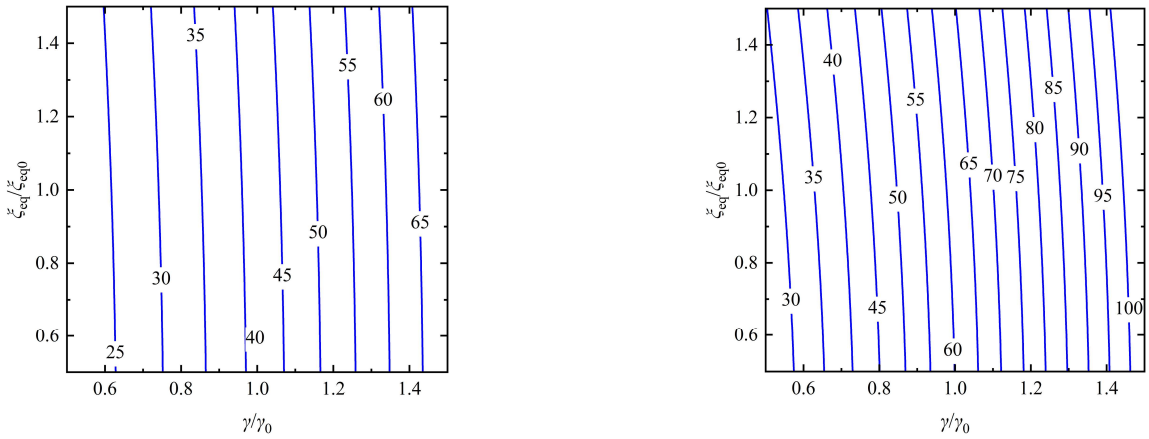

(a) $\mu = 0.01$, $\mu_{vs} = 0.05$. **(b)** $\mu = 0.01$, $\mu_{vs} = 0.1$.

Figure 5. Influences of active parameters on the stroke of HMD. **(a)** ξ_{eq}/ξ_{eq0} with $\mu = 0.01$, $\mu_{vs} = 0.05$; **(b)** ξ_{eq}/ξ_{eq0} with $\mu = 0.01$, $\mu_{vs} = 0.1$.

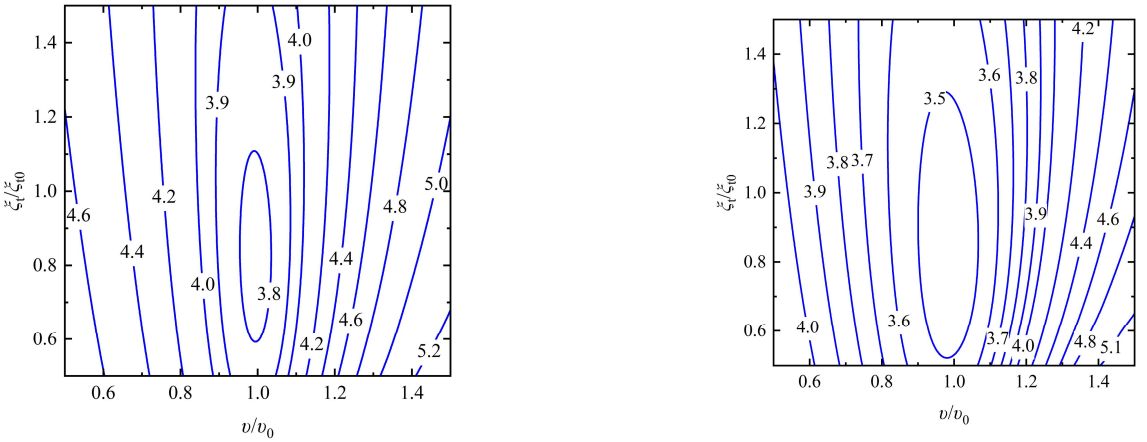

(a) $\mu = 0.01$, $\mu_{vs} = 0.05$. **(b)** $\mu = 0.01$, $\mu_{vs} = 0.1$.

Figure 6. Influences of passive parameters on the structural response. **(a)** ξ_t/ξ_{t0} with $\mu = 0.01$, $\mu_{vs} = 0.05$; **(b)** ξ_t/ξ_{t0} with $\mu = 0.01$, $\mu_{vs} = 0.1$.

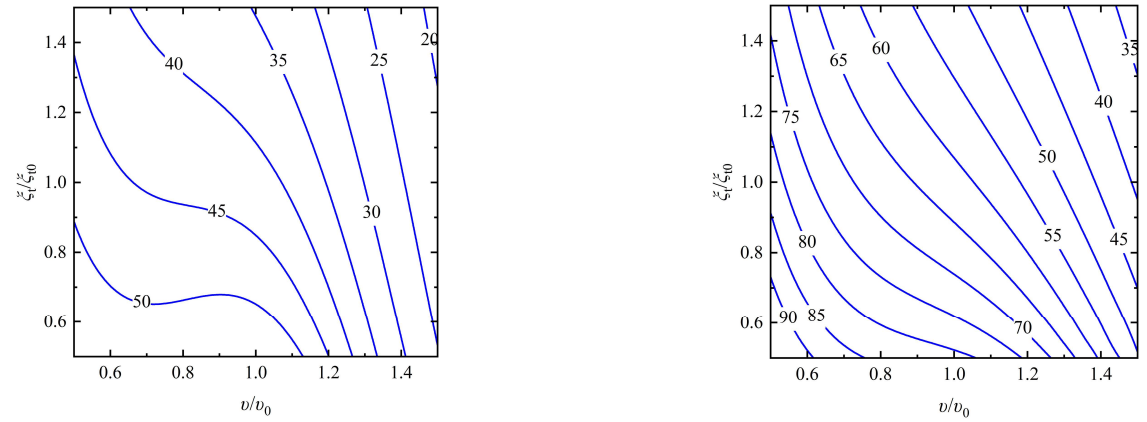

(a) $\mu = 0.01$, $\mu_{vs} = 0.05$. **(b)** $\mu = 0.01$, $\mu_{vs} = 0.1$.

Figure 7. Influences of passive parameters on the stroke of HMD. **(a)** ξ_t/ξ_{t0} with $\mu = 0.01$, $\mu_{vs} = 0.05$; **(b)** ξ_t/ξ_{t0} with $\mu = 0.01$, $\mu_{vs} = 0.1$.

The values on the contour lines in **Figures 4–7** represent k_s times the area of the transfer function, and the parameters on the coordinate axis are as follows.

$$\upsilon_0 = \frac{1}{1+\mu}, \xi_{t0} = \sqrt{\frac{3\mu}{8(1+\mu)^3}}, \gamma_0 = \frac{\sqrt{\mu_{vs}-\mu}}{1+\mu_{vs}}, \xi_{eq0} = \sqrt{\frac{3\mu_{vs}(\mu_{vs}-\mu)}{8(1+\mu_{vs})^3}} \tag{11}$$

It can be seen in **Figures 4** and **5** that the structural response and HMD stroke basically do not change with the variation of ξ_{eq}, while almost linear variation with γ. As **Figures 6** and **7** shown, the structural response has an optimal value and the structural response changes little near the optimal value, while the HMD stroke changes a lot with the variation of υ and ξ_t. It is worth noting that near the optimal value of structural response, the structural response almost keeps unchanged, while the HMD stroke changes a lot. Therefore, it can be achieved by weighting and optimizing the structural response and HMD stroke without significantly changing the control effect in structural response.

In order to weight the structural response and HMD stroke, this article normalized the structural response and HMD stroke, and then weighted them in the performance index function as follows.

$$J_{ij} = C_s \frac{A_{s,ij}}{\sum A_{s,ij}} + C_t \frac{A_{t,ij}}{\sum A_{t,ij}}, C_s + C_t = 1 \tag{12}$$

where, C_s and C_t are the weighted coefficients of structural response and HMD stroke respectively, $A_{s,ij}$ and $A_{t,ij}$ are the k_s times the area of the transfer function of structural response and HMD stroke respectively when $\upsilon = \upsilon_i$, $\xi_t = \xi_{t,i}$.

When the weighted coefficients of structural response and HMD stroke are 0.9 and 0.1 respectively, the optimized results after weighting are displayed in **Figures 8–10**. **Figure 8** is the optimized results of performance index function with different passive parameters, the optimal parameters for HMD are the parameters corresponding to the minimum value in **Figures 8–10** give the amplitudes of structural responses and strokes with TMD control, unoptimized HMD (UHMD) control and optimized HMD (OHMD) control under the optimal situation considering the balance of structural response and stroke of HMD. The parameters of UHMD are calculated using Equation (11).

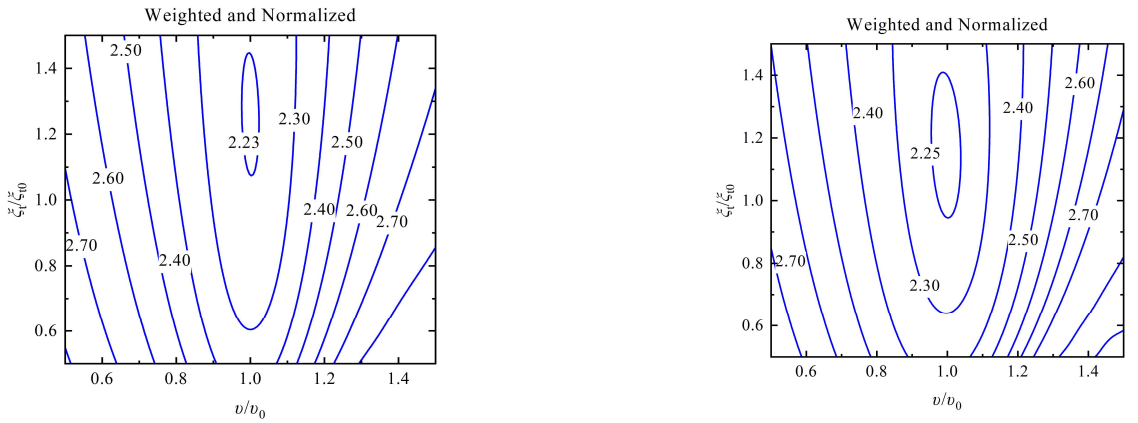

(a) $\mu = 0.01$, $\mu_{vs} = 0.05$. **(b)** $\mu = 0.01$, $\mu_{vs} = 0.1$.

Figure 8. Influences of passive parameters on performance index function ($\times 10^{-5}$). **(a)** ξ_t/ξ_{t0} with $\mu = 0.01$, $\mu_{vs} = 0.05$; **(b)** ξ_t/ξ_{t0} with $\mu = 0.01$, $\mu_{vs} = 0.1$.

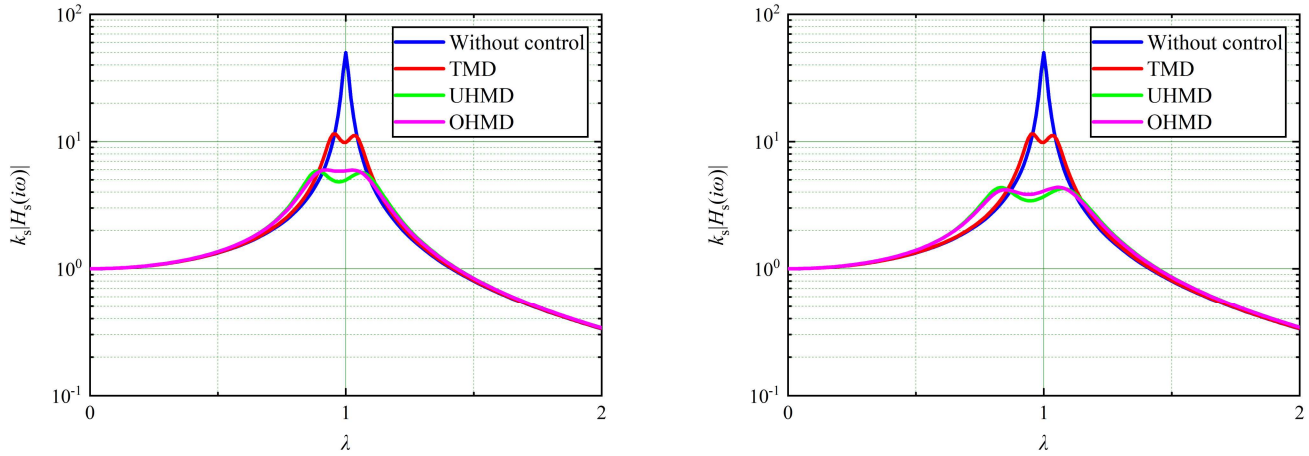

(a) $\mu = 0.01$, $\mu_{vs} = 0.05$. **(b)** $\mu = 0.01$, $\mu_{vs} = 0.1$.

Figure 9. Amplitudes of TMD, UHMD and OHMD controlled SDOF structural responses. **(a)** $k_s|H_s(i\omega)|$ with $\mu = 0.01$, $\mu_{vs} = 0.05$; **(b)** $k_s|H_s(i\omega)|$ with $\mu = 0.01$, $\mu_{vs} = 0.1$.

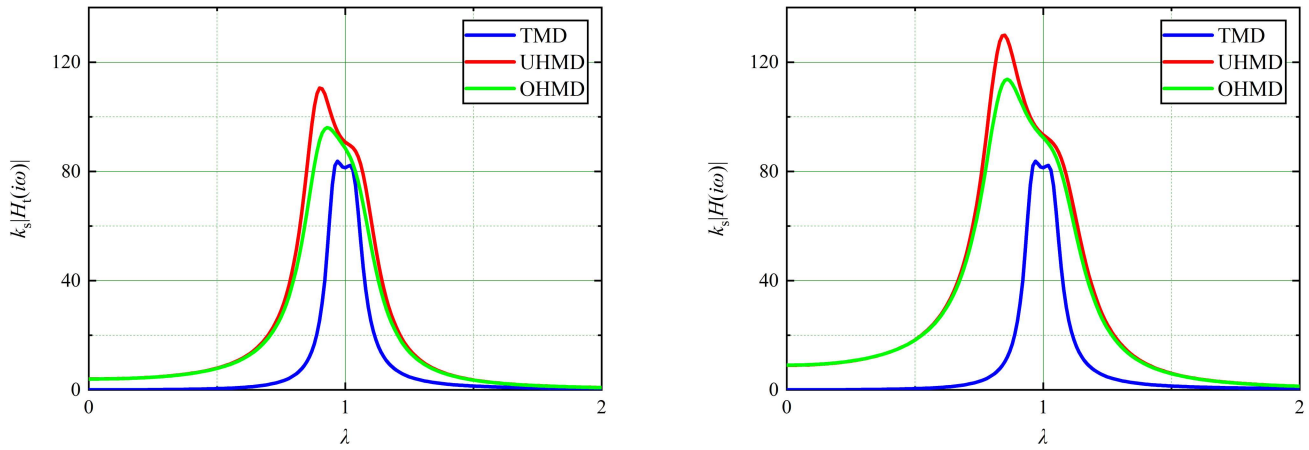

(a) $\mu = 0.01$, $\mu_{vs} = 0.05$. **(b)** $\mu = 0.01$, $\mu_{vs} = 0.1$.

Figure 10. Amplitudes of TMD, UHMD and OHMD strokes. **(a)** $k_s|H_t(i\omega)|$ with $\mu = 0.01$, $\mu_{vs} = 0.05$; **(b)** $k_s|H_t(i\omega)|$ with $\mu = 0.01$, $\mu_{vs} = 0.1$.

From the optimized results in **Figures 9** and **10**, it can be seen that the control effect of OHMD is slightly decreased but not significantly decreased compared UHMD, while the stroke of OHMD is lower than that of UHMD. When $\mu = 0.01$, $\mu_{vs} = 0.05$ or 0.1, the control effect of OHMD decreased by 1.0% and 0.6% compared to UHMD, while the stroke of HMD decreased by 9.6% and 5.8%. That is to say, weighting and optimizing the structural response and HMD stroke is a feasible optimization method for HMD based on virtual TMD without sacrificing too much control performance.

4. Numerical example

The previous chapter optimized the HMD by weighting the structural response and HMD stroke, reducing the stroke of the HMD without significantly changing the control effect, and verified the feasibility of the optimization in the frequency domain.

This chapter uses the optimization method from the previous section to optimize the HMD and verifies its control performance in the time domain.

Considering a SDOF structure with fundamental frequency f_s = 0.2 Hz and with damping ratio ξ_s = 1%. The load for SDOF structure is the Gaussian white-noise load with a standard deviation of 0.1 and a mean value of 0. The load time-history and its power spectral density (PSD) are displayed in **Figure 11**. The dynamic equation of the SDOF structure is:

$$\ddot{x} + 2\xi_s\omega_s\dot{x} + \omega_s^2 x = p \tag{13}$$

where, $\omega_s = 2\pi f_s$, p represents the random load.

Rewriting Equation (13) into state space equation.

$$\dot{Z} = AZ + Dp, Z = \{x \quad \dot{x}\}^T, A = \begin{bmatrix} 0 & 1 \\ -\omega_s^2 & -2\xi\omega_s \end{bmatrix}, D = \begin{Bmatrix} 0 \\ 1 \end{Bmatrix} \tag{14}$$

The state space equation of the controlled SDOF structure is:

$$\dot{Z} = AZ + Bu + Dp, B = \{0 \quad 1\}^T \tag{15}$$

where, u is the control force of control device acting on the SDOF structure.

The weighted coefficients of structural response and HMD stroke are 0.9 and 0.1 respectively. In addition, in order to reduce the random errors in the calculation process, this paper simulated the responses of SDOF structure under 10 different random loads, as well as the control performance and stroke of HMD devices. the simulation results are given in **Figures 12–18** and **Table 1**.

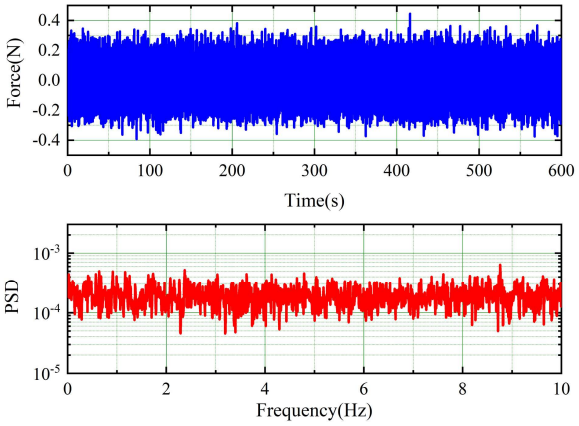

Figure 11. Load time-history and its PSD.

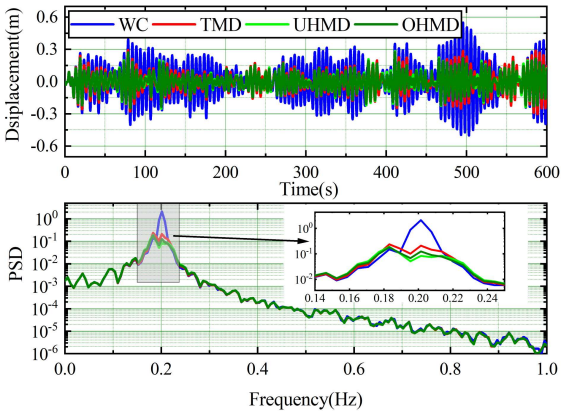

Figure 12. Displacement time-history and its PSD.

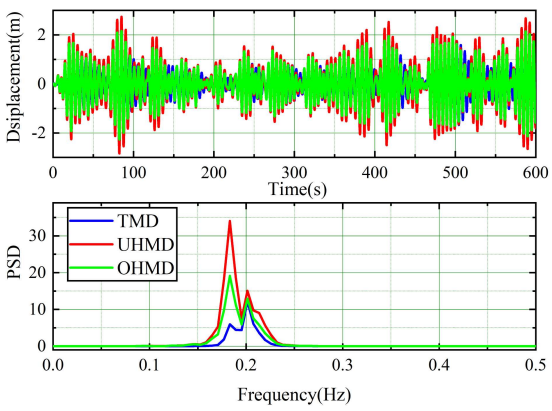

Figure 13. Stroke time-history and its PSD.

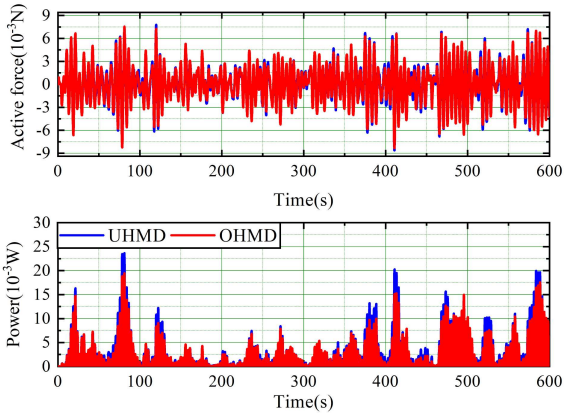

Figure 14. Active control force and power.

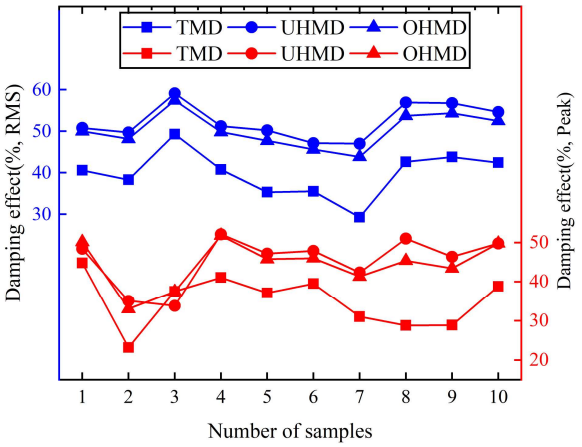

Figure 15. Displacement damping effects.

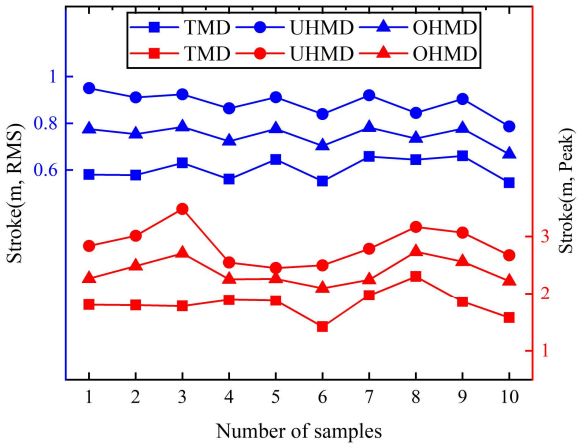

Figure 16. Strokes of control devices.

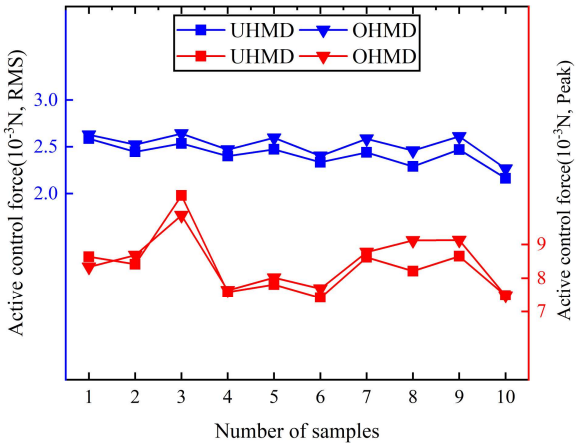

Figure 17. Active control force of UHMD and OHMD.

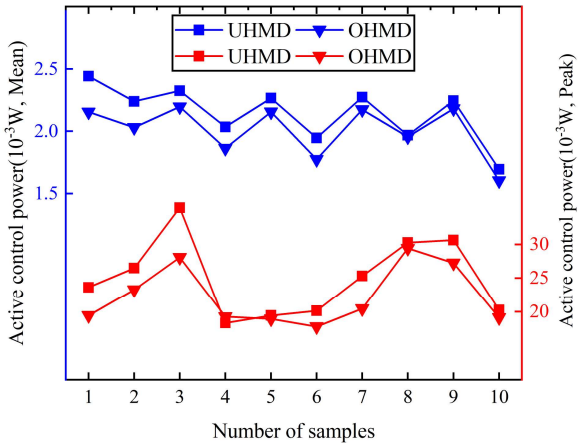

Figure 18. Active control power of UHMD and OHMD.

Table 1. Control performances of TMD, UHMD and OHMD.

	Displacement (m)		**Stroke (m)**		**Active control force (10^{-3} N)**		**Active control power (10^{-2} W)**	
	Average RMS	**Average Peak**	**Average RMS**	**Average Peak**	**Average RMS**	**Average Peak**	**Average Mean**	**Average Peak**
WC	0.168	0.502	-	-	-	-	-	-
TMD	0.100	0.329	0.606	1.826	-	-	-	-
UHMD	0.079	0.273	0.886	2.854	2.413	8.329	0.214	2.499
OHMD	0.083	0.278	0.748	2.385	2.518	8.473	0.201	2.231

Figures 12 and **13** display the structural displacement time-history and stroke time-history of without-controlled (WC), TMD controlled, UHMD controlled and OHMD controlled SDOF structures under one sample load. **Figures 15** and **16** summarize the root mean square (RMS) and peak values of structural displacement and stroke under 10 sample loads. From the results, it can be seen that the control effect of OHMD is better than TMD and almost the same as UHMD, while the stroke of OHMD is much lower than UHMD. The average control effects in RMS values of UHMD and OHMD controlled structural displacements are 53.0% and 50.6% respectively, and average control effects in peak values of UHMD and OHMD

controlled structural displacements are 45.6% and 44.6% respectively. **Figure 14** gives the active control force and power time-histories of UHMD and OHMD. **Figure 17** shows the RMS and peak values of active control forces of UHMD and OHMD and **Figure 18** exhibits the mean and peak values of active control powers of UHMD and OHMD. The active control force of OHMD is much higher than UHMD, while the active control power of OHMD is much lower than UHMD.

Generally speaking, the control effect of OHMD loses 2.4% in RMS value and 0.8% in peak value compared to UHMD, while the stroke of OHMD reduces 15.6% in RMS value and 16.4% in peak value compared to UHMD. The active control force of OHMD increases 4.4% in RMS value and 1.7% in peak value compared to UHMD, while the active control power of OHMD decreases 6.1% in mean value and 10.7% in peak value compared to UHMD. The comprehensive control performance of OHMD is better than UHMD. That is to say, the optimization of HMD through weighting the structural response and stroke is feasible. This optimization method can improve the comprehensive control performance of HMD without significantly reducing the control effect.

5. Conclusion

This paper proposed a hybrid control algorithm based on virtual TMD and verified its feasibility through frequency domain analysis, and then optimized the parameters of HMD by weighting the structural response and stroke to improve the comprehensive control performance. In order to further demonstrate the comprehensive control performance of the optimized HMD, this paper conducted time history analysis under 10 different white noise random loads. The simulation results demonstrated that the optimized HMD has a better comprehensive control performance than the unoptimized HMD. The main conclusions are as follows.

1) HMD based on virtual TMD control algorithm can achieve excellent control effect than passive TMD with large mass ratio (≥5%) in the premise of unchanging the actual physical mass of the control device.

2) Without changing the original control effect, by replacing some of the active control force with stiffness and damping, the active control force of HMD can be further reduced.

3) After weighting and optimizing the structural response and HMD stroke, although the control effect of HMD is slightly reduced, the HMD stroke is also significantly reduced. Overall, the comprehensive control performance of the optimized HMD has been improved.

Author contributions: Conceptualization, YY and QW; methodology, YY; software, YY; validation, YY, QW and QY; formal analysis, YY; investigation, YY, QW and TL (Tao Long); resources, QW; data curation, YY; writing—original draft preparation, YY and QW; writing—review and editing, YY, QW, QY, TL (Tian Li) and GQ; visualization, YY; supervision, QW, QY, TL (Tian Li) and GQ; project administration, QW; funding acquisition, QW, QY, TL (Tian Li) and GQ. All authors have read and agreed to the published version of the manuscript.

Funding: This research was funded by the National Natural Science Foundation of

China, Grant No. (52008061, 567890 and 42002293), Hainan Provincial Key R&D Program, Grant No. (ZDYF2022SHFZ353-06) and the China Postdoctoral Science Foundation, Grant No. (2020M673138).

Conflict of interest: The authors declare no conflict of interest.

References

1. Pourzeynali S, Lavasani HH, Modarayi AH. Active control of high rise building structures using fuzzy logic and genetic algorithms. Engineering Structures. 2007; 29(3): 346–357. doi: 10.1016/j.engstruct.2006.04.015
2. Frahm H. Device for damping vibrations of bodies. U.S. Patent 0989958, 18 April 1911.
3. Tsai H, Lin G. Optimum tuned-mass dampers for minimizing steady-state response of support-excited and damped systems. Earthquake Engineering & Structural Dynamics. 1993; 22(11): 957–973. doi: 10.1002/eqe.4290221104
4. Rana R, Soong TT. Parametric study and simplified design of tuned mass dampers. Engineering structures. 1998; 20(3): 193–204. doi: 10.1016/S0141-0296(97)00078-3
5. Murtagh PJ, Ghosh A, Basu B, et al. Passive control of wind turbine vibrations including blade/tower interaction and rotationally sampled turbulence. Wind Energy. 2007; 11(4): 305–317. doi: 10.1002/we.249
6. Kim Y, You K, You J. Passive control of along-wind response of tall building. Journal of Central South University. 2014; 21(10): 4002–4006. doi: 10.1007/s11771-014-2388-3
7. Dinh VN, Basu B. Passive control of floating offshore wind turbine nacelle and spar vibrations by multiple tuned mass dampers. Structural Control and Health Monitoring. 2014; 22(1): 152–176. doi: 10.1002/stc.1666
8. You KP, You JY, Kim YM. LQG Control of Along-Wind Response of a Tall Building with an ATMD. Mathematical Problems in Engineering. 2014; 2014: 1–7. doi: 10.1155/2014/206786
9. Fitzgerald B, Sarkar S, Staino A. Improved reliability of wind turbine towers with active tuned mass dampers (ATMDs). Journal of Sound and Vibration. 2018; 419: 103–122. doi: 10.1016/j.jsv.2017.12.026
10. Cong C. Using active tuned mass dampers with constrained stroke to simultaneously control vibrations in wind turbine blades and tower. Advances in Structural Engineering. 2018; 22(7): 1544–1553. doi: 10.1177/1369433218817892
11. Hrovat D, Barak P, Rabins M. Semi-active versus passive or active tuned mass dampers for structural control. Journal of Engineering Mechanics. 1983; 109(3): 691–705. doi: 10.1061/(ASCE)0733-9399(1983)109:3(691)
12. Nagarajaiah S, Varadarajan N. Short time Fourier transform algorithm for wind response control of buildings with variable stiffness TMD. Engineering Structures. 2005; 27(3): 431–441. doi: 10.1016/j.engstruct.2004.10.015
13. Sun S, Yang J, Du H, et al. Development of magnetorheological elastomers–based tuned mass damper for building protection from seismic events. Journal of Intelligent Material Systems and Structures. 2018; 29(8): 1777–1789. doi: 10.1177/1045389x17754265
14. Yang Q, Yang Y, Wang Q, et al. Study on the fluctuating wind responses of constructing bridge towers with magnetorheological elastomer variable stiffness tuned mass damper. Journal of Intelligent Material Systems and Structures. 2021; 33(2): 290–308. doi: 10.1177/1045389x211014574
15. Wang L, Zhou Y, Shi W. Seismic Response Control of a Nonlinear Tall Building Under Mainshock–Aftershock Sequences Using Semi-Active Tuned Mass Damper. International Journal of Structural Stability and Dynamics. 2023; 23(16n18). doi: 10.1142/s0219455423400278
16. Wang L, Nagarajaiah S, Zhou Y, et al. Experimental study on adaptive-passive tuned mass damper with variable stiffness for vertical human-induced vibration control. Engineering Structures. 2023; 280: 115714. doi: 10.1016/j.engstruct.2023.115714
17. Wang L, Zhou Y, Shi W. Random crowd-induced vibration in footbridge and adaptive control using semi-active TMD including crowd-structure interaction. Engineering Structures. 2024; 306: 117839. doi: 10.1016/j.engstruct.2024.117839
18. Li C, Cao B. Hybrid active tuned mass dampers for structures under the ground acceleration. Structural Control and Health Monitoring. 2014; 22(4): 757–773. doi: 10.1002/stc.1716
19. Collette C, Chesné S. Robust hybrid mass damper. Journal of Sound and Vibration. 2016; 375: 19–27. doi: 10.1016/j.jsv.2016.04.030
20. Hsieh MC, Huang GL, Liu H, et al. A numerical study of hybrid tuned mass damper and tuned liquid damper system on structure motion control. Ocean Engineering. 2021; 242: 110129. doi: 10.1016/j.oceaneng.2021.110129